Measuring the administered dose of particles on the facial mucosa of a realistic human model

Duan, Mengjie; Liu, Li; Da, Guillaume; Géhin, Evelyne; Nielsen, Peter V; Weinreich, Ulla M; Lin, Borong; Wang, Yi; Zhang, Ting; Sun, Wei

Published in:
Indoor Air

DOI (link to publication from Publisher):
10.1111/ina.12612

Publication date:
2020

Document Version
Accepted author manuscript, peer reviewed version

DR. LI LIU (Orcid ID : 0000-0001-8512-8676)

Article type : Original Article

Measuring the administered dose of particles on the facial mucosa of a realistic human model

Mengjie Duan[1,2], Li Liu[1,3,4,*], Guillaume Da[2], Evelyne Géhin[2], Peter V. Nielsen[4], Ulla Weinreich[5,6], Borong Lin[1], Yi Wang[3,7], Ting Zhang[8], Wei Sun[8]

1Department of Building Science, School of Architecture, Tsinghua University, Beijing, China

2Université Paris-Est, CERTES (EA 3481), UPEC, Créteil, France

3State Key laboratory of Green Building in Western China, Xi'an University of Architecture and Technology, Xi'an, China

4Department of Civil Engineering, Aalborg University, Aalborg, Denmark

5Department of Respiratory Diseases, Aalborg University Hospital, Aalborg, Denmark

6The Clinical Institute, Aalborg University, Aalborg, Denmark

7School of Building Services Science and Engineering, Xi'an University of Architecture and Technology, Xi'an, China

8Biomanufacturing Center, Department of Mechanical Engineering, Tsinghua University, Beijing, China

Corresponding to Li Liu, liuli_archi@tsinghua.edu.cn

Practical Implications

Increased exposure to particulate contaminants has been linked to deleterious health and well-being outcomes. This study provides an in vitro method to quantify the administered dose of

This article has been accepted for publication and undergone full peer review but has not been through the copyediting, typesetting, pagination and proofreading process, which may lead to differences between this version and the Version of Record. Please cite this article as doi: 10.1111/INA.12612

particulates deposited on the facial mucosa on an individual basis. With the merits of low cost and timely processing, this method enlightens the future design of personalized environment control and protection strategies.

Acknowledgment

This work was supported by the National Key Research and Development Program of China (Grant No. 2017YFC0702700) and the National Natural Science Foundation of China (Grant No. 51778520).

None of the authors declares any conflict of interest.

Abstract

Exposure to particulate contaminants can cause serious adverse health effects. Deposition on the facial mucosa is an important path of exposure, but it is difficult to conduct direct dose measurement on real human subjects. In this study, we propose an in vitro method to assess the administered doses of micron-sized particles on the eyes and lips in which computed tomographic scanning and three-dimensional printing were used to create a model that includes a face, oropharynx, trachea, the first five generations of bronchi, and lung volume. This realistic model of a face and airway was exposed to monodispersed fluorescent particles released from an incoming jet. The administered dose of particles deposited upon the eyes and lips, as quantified by fluorescence intensity, was determined via a standard wiping protocol. The results show that, in this scenario, the administered doses normalized by source were 2.15%, 1.02%, 0.88%, 2.13%, and 1.55% for 0.6-μm, 1.0-μm, 2.0-μm, 3.0-μm, and 5.0-μm particles, respectively. The administered dose of large particles on the mucosa within a given exposure time has great significance. Moreover, the lips suffer a much greater risk of exposure than the eyes and account for more than 80% of total facial mucosa deposition. Our study provides a fast and economical method to assess the administered dose on the facial mucosa on an individual basis.

Key words: mucosal exposure; in vitro; CT scanning; 3D printing; deposition; occupational health

1. Introduction

Public and occupational exposure to particulate contaminants is considered a common

threatening factor to human health[1,2]. Deposition on the mucosa, along with inhalation and deposition on the skin, is a major pathway for intake of particles into the body, which may result in a series of adverse health outcomes, such as irritation, inflammation, and chronic disease[3–6]. Intact skin poses an effective barrier against the absorption of particles, but the thin epidermal layers of mucosal surfaces are less protective. Epidemiologic studies have reported that burning, dryness, and itching of the eyes are among the most common symptoms from occupant complaints[7,8]. Prolonged exposure to environmental particulate pollution can cause severe disease[9,10]. An accurate and quantitative measure of the causal relationship between exposure and health outcomes would certainly benefit the development of effective control strategies, but such a measure is beyond the resolution of common epidemiologic studies. In vitro methods[11,12] such as cell[13] or animal models[14,15] can implement partial pathological evidence of damage to genes, tissues, and organs, but their lack of individual susceptibility limits definitive conclusions for population subgroups. In contrast, biomarkers that indicate oxidative stress, inflammation, thrombosis, and many other health outcomes reflect individual susceptibility[16,17], but uncertainty remains due to disturbances from uncontrolled confounders. Nevertheless, decades of medical studies have supplied massive evidence for exposure limits to particulate contaminants, especially in occupational scenarios. For instance, exposure to household and ambient fine particulate matter ($PM_{2.5}$) should not exceed 5.9 $\mu g/m^3$ for a theoretical minimum health risk[1]. The exposure in practice is often interpreted as the spatial average of local particle concentrations at chosen sampling locations or as the temporal average of total particle counts obtained near body intake pathways. Neither measure is equivalent to the dose of particles administered to the facial mucosa or to the associated health outcomes due to factors such as the deposition efficiency, the proximity to the contaminant source, and the particle distribution in room air[3].

Until recent years, it was impossible to measure the administered dose, that is, the number of particles that make direct contact with the body's absorption barriers and are therefore available for absorption. For respiratory issues, individual in vitro models[18,19] have been constructed to simulate the dose of particles administered to anatomically correct airways with a fast-developing computed tomographic (CT) technique[20–23]. These models make it feasible to assess the dose on an

individual basis, which parallels the need for personalized environment control strategies[24]. In addition to evidence from medical studies, an assessment of the actual administered dose would benefit our understanding of the causal relationships among exposure, the dose, and the associated health outcomes. However, studies that have used anatomically correct models have focused mainly on inhalation[25–28]. We were unable to find a mucosa dose assessment based on an in vitro model.

In this study, a new method is proposed to assess the administered dose on human facial mucosa. Based on CT images from a healthy volunteer, a realistic face and airway model that included a face, an oropharynx, a trachea, the first five generations of bronchi, and lung volume was obtained via three-dimensional (3D) printing and connected to a pump to simulate steady-state inhalation. Micron-sized monodispersed fluorescent particles were generated by TSI VOAG 3450 and monitored by TSI APS 3321. Administered doses on eyes and lips were quantified as the cumulative deposition mass, as measured via a wiping method and calculated via fluorescence intensity-mass concentration correlation curves. This in vitro method provides a fast and economic means to assess administered dose on facial mucosa.

2. Methods

2.1 In vitro face and airway model

An in vitro model replicates only a portion of human physiologic functions. In this study, the model represented the detailed geometry of the face and airway. The geometry was obtained by processing the CT images of a healthy 34-year-old male volunteer with no history of smoking or lung disease. Imaging was conducted in the supine position with a Philips Brilliance iCT scanner (Koninklijke Philips N.V., Netherlands). The obtained data were helical with reconstructed axial slices 1.5 mm thick; and 560 two-dimensional slices covered the geometry from head to diaphragm (Figure 1a and 1b). The regions of interest were identified and extracted with commercial software (Materialise Mimics 17.0, Ann Arbor, MI). The current imaging resolution allows modeling up to the fifth generation of bronchi. The terminal bronchi were trimmed along planes normal to the centerline, where the airflow enters the lung volume formed by the lungs' boundary. Figure 1c shows the extracted geometry.

A realistic face and airway model was printed via the stereolithographic appearance 3D printing technique. A photosensitive resin SPR6000 was used (XJRP, Xi'an, China), with a surface roughness of less than 0.1 mm and an electrostatic capacitance of less than 0.002 μC (<0.4 m/s flow speed; 25°C, 50% relative humidity). The model was printed in three parts: the face with the central airway; the left lung volume with G1-G5 left upper lobe and left lower lobe; and the right lung volume with G1-G5 right upper lobe, right middle lobe, and right lower lobe. For sampling and cleaning purposes, the left and right lung volumes were designed to be separated into two parts, both of which can be connected and sealed externally to become airtight. Figure 2 shows the face and airway model under sealed and separated conditions.

The thickness of the model boundary was 3.0 mm. One 5.0-mm conducting tube was added to the outer side of each lung volume, respectively, to connect with the pump to generate the inhalation airflow. Figure 2 shows the 5.0-mm sampling hole added to the bottom of each lung volume.

The financial and time costs to make such a model are low, so it is feasible to conduct a series of measurements or numerical simulations for a population subgroup. This study used one individual case to illustrate the procedure of measurement and result analysis.

2.2 Experimental setup

The experiment was conducted in a ventilation cabinet (1.8 × 0.7 × 1.4 m). The ventilation system was run to exhaust any particles before each trial. Figure 3 presents detailed information on the experimental setup. A monodispersed particle jet was generated continuously with a vibrating orifice aerosol generator model (VOAG 3450, TSI, USA). A liquid solution of ultrapure water and sodium fluorescein ($C_{20}H_{10}Na_2O_5$) was injected into the VOAG with a syringe pump at a predetermined volume flow rate. The solution jet was released through a small orifice (diameter, 20 μm). The jet breaks up into uniform droplets when the orifice vibrates, and the size of the droplets generated was dependent on the operating frequency and the syringe pump flow rate. For this measurement, the orifice operating frequency ranged from 67.0 to 75.0 kHz, and the syringe pump flow rate ranged from 8.3 to 12.0 mL/h. We generated 0.6-μm, 1.0-μm, 2.0-μm, 3.0-μm, and 5.0-μm monodispersed particles that were totally evaporated from the initial monodispersed

droplets in a drying cylinder. The particle density was 1530 kg/m^3. The circular opening of the cylinder carries the airflow jet and the particles toward the model of the face and airway.

The Aerodynamic Particle Sizer Spectrometer Model APS 3321 (TSI, USA) was used to monitor the particulate size distribution and concentration in real time. The monodispersity of the particle size ranged from 78.5% to 93.3%, and the geometric standard deviation was less than 1.2. After the concentration stabilized, the spectrometer was disconnected, and the model was put inside the cabinet. The distance from the nose of the model to the outlet of the particle jet was kept as 0.2 m. A mouth-breathing man was simulated during the measurement when the nose was well sealed. The model can mimic patients with symptoms such as a runny nose or workers performing heavy exercise[29]. The continuous inhalation airflow of 11.0 ± 1.0 L/min provided by the vacuum pump was similar to the standard flow rate of a man while standing[30]. The vacuum pump was connected to the outlets on both sides of the lungs. The administered doses of eyes and lips were represented as the accumulated mass of particles deposited on the target surface during the exposure time. The ventilation system was turned off during the measurements. Trials for each particle size were repeated three times to obtain an average value.

2.3 Wiping method and verification

Administered doses on left eye, right eye, and lips were quantified via the wiping method developed by Da et al.[31]. Fluorescent particles on the target regions were wiped more than five times with cotton buds humidified in 20 cm^3 of water (1:1000 of 20% liquid ammonia in ultrapure water) and transferred into samplers. This process was repeated three times per case for each sampling region. The fluorescence intensity was detected with a fluorophotometer Fluoro Max-4 (Horiba, Japan), and the particle mass was calculated on the basis of the calibrated relationship between the fluorescence intensity and the mass concentration (Figure 4). The total mass of three repeated samples was the administered dose for the target region.

The efficiency of the wiping method was quantified on the basis of the particle transfer loss rate. A certain amount of sodium fluorescein was weighed with a high-precision balance (Satorius MC210P, Germany) and dissolved into the ammonia solution. A fixed volume of fluorescent solution was then dropped onto a sample surface of the same material as the model. After natural

drying of fluorescent solution in a clean environment, the fluorescence intensity was measured, and the particle transfer loss rate was calculated as 44.4% ± 6.7%, which indicates a high rate of particulate adhesion on the material surface. We therefore used aluminum foil, which has excellent collection efficiency and low static electricity to cover the eyes and lips (Figure 2), which limited the transfer rate loss to 12.5% ± 5.2%.

Our study focuses on exposure to monodispersed fine particles with aerodynamic diameters of 0.6, 1.0, 2.0, 3.0, and 5.0 μm. Because the fluorescence intensity increased with the particle mass and size, we extended the exposure time for smaller particles to facilitate the collection of samples within the range of a standard curve. Table 1 shows the experimental levels for each particle size.

2.4 Method uncertainty

To the best of our knowledge, no published studies have measured the administered dose on the eyes and lips of real human subjects. We were thus unable to calibrate our in vitro model with a quantitative in vivo method, if any exists. The major limitation of our model is its obvious lack of biological properties of real human subjects.

2.4.1 Eyelashes

Real-time monitoring to quantify the actual dose in human subjects presents a challenge, so compromises were necessary during the study design process. Our method did not consider eyelashes or blinking, which may have greatly reduced the actual doses. The limited availability of human eyelids for sampling means that studies remain scarce despite recent advances in eyelash research[32]. No in vivo studies of human eyelash aerodynamics have yet been published. Only one study has applied an in vitro method to explore in detail the aerodynamic features around the eyes[33]. In that study, the model geometry was idealized into an ocular surface with surrounding eyelashes and was isolated from the rest of the body. To determine the eyelashes' effects on deposited particles, fluorescent droplets with an average size of 10 μm were injected with a commercial humidifier. An absorbent paper disc was applied to the ocular surface to intercept incoming droplets. The fluorescence intensity corresponded to the number of droplets deposited. Five eyelash lengths L were used, and the ratios of the eyes' width W to the length of the eyelashes

were measured as 0.0 (without eyelashes), 0.1, 0.2, 0.4, and 0.8. Table 2 lists the relationship between L/W and the fluorescence intensity.

The human eyelash normally ranges from 8.0 to 12.0 mm long[34]. The average eye width of the volunteer in our study was 26.7 mm. Amador et al. found that the administered doses of 10.0-μm particles will be overestimated by 25% to 40% in mammals if the eyelashes are neglected.

2.4.2 Mucosal lining fluid

Our model did not include goblet cells, mucus secretory cells, or submucosal glands to produce mucosal lining fluid (i.e., mucus)[35]. Mucin is the main structural component of mucus; these components interact with each other and with other components of mucus to form a meshlike structure[12,36,37]. In addition to this meshlike structure, mucus captures foreign particles via an adhesion effect. However, the density, viscosity, and elasticity of human mucus are not evident in the literature, not to mention the mucin-based meshlike structure within it. As a result, we were unable to find any valid simulant. Moreover, some studies[38,39] have suggested that the efficient defense proteins in saliva near the mucosal surfaces of the oral cavity contribute to inhibit influenza viruses. Whether the mucin from real-life mucus plays a role in defending against illness, infection, and/or poisoning requires further investigation. In addition, the main component of mucus is water (up to 95% by weight), so the wetting of real mucosa differs from that in our in vitro model. By neglecting mucus, we were unable to mimic the humid environment along the mucosa's boundary layer, which adds uncertainty to the deposition of hygroscopic particles[40].

2.4.3 Body heat release

Our method simplifies the exposure process into an isothermal scenario. The temperature of the model's skin was 6°C to 10°C lower than that of human skin. The consequent variation in thermophoresis on micron-sized particles is negligible[41]. Nevertheless, when in a state of thermal comfort, the human body dissipates 30% to 35% of its metabolic heat via convection. The human convective boundary layer (i.e., the body plume) interacts with the surrounding airflows and modifies their movement around the human microenvironment [42]. The body plume can entrain particles from the ambient air into the breathing zone[43–45], where the plume velocity can reach

0.15 to 0.30 m/s. In our study, the particle-laden jet had an initial velocity of 0.94 m/s. The centerline velocity decreased to about 0.86 m/s when the jet met the model, as estimated with the free jet theory[46]. The jet's momentum is much stronger than that of the plume flow, so we ignored heat release under the current measurement setup. It should be noted that the plume flow plays an important role in exposure when source of contamination is sufficiently near.

2.4.4 Blank measurement

In addition to neglecting the biological features of real human subjects, we also estimated the uncertainty induced by measurement with the fluorescent tracer. We measured the differences in intensity before and after exposure to pure water droplets to evaluate the influence of background particles. The experimental setup was the same as shown in Figure 3. The presence of only a slight difference in Figure 5 indicates that the deposition of environmental particles can be neglected.

The fluorescence that remains on the surface after each test will increase the uncertainty. We thus cleaned the model by immersing it in a tank filled with a mixture of pure water and detergent for 24 hours and measured the intensity of the eyes and lips before each trial. The fluorescence intensity of the auxiliary solution (i.e., pure water and ammonia) was also tested to exclude any influence on the fluorescent solution. The results are shown in Figure 6 and were used as a benchmark for the experiments' reliability. If the fluorescence intensity of each measurement was one magnitude greater than the background, the fluorescent residue was considered to have little effect on the experimental results.

3. Results

3.1 Mucosal deposition

The mucosal exposure ratio is defined by the ratio of the administered dose w_i in the total source release w_0.

$$w_0 = C_s \cdot q \cdot \Delta t \cdot V_p \tag{2}$$

Where

w_0, total source release (g);

C_S, particle concentration at the opening of the jet flow (N/m^3);

q, inhalation airflow rate (m^3/s);

Δt, total exposure time (s);

V_p, particulate volume (m^3).

Administered doses of eyes and lips were normalized by the total source release (Figure 7). As shown in Figure 8, the mucosal deposition rate ranged from 2.13% ± 0.63% to 0.88% ± 0.56% (g/g) for 0.6-μm to 5.0-μm particles, and the 0.6-μm, 3.0-μm, and 5.0-μm particles showed a high mucosal deposition rate due to the relaxation time of the various size particles. A longer relaxation time makes larger particles easier to separate with airflow during transportation than smaller particles, and it means that they are less likely to be inhaled and deposited on the surface. The opposite is true for smaller particles. Hence, the smallest and largest particles both resulted in a high dose to the facial mucosa.

Figure 8 also indicates the distribution of particle deposition on the eyes and lips. We conclude that the lips contribute to more than 80% of the administered dose to the total facial mucosa for particles between 0.6 and 5.0 μm. We suspect that the lips' large surface area relative to the eyes is the reason for the high administered dose. The effects of surface area on the left eye, right eye, and lips are discussed further below.

3.2 Individual difference assessment

The administered dose index AD_i named as particle deposit on unit surface in unit time (Eq. 3).

$$AD_i = \frac{w_i}{A \cdot \Delta t} \quad (mg/m^2 \cdot s) \tag{3}$$

Where A is the area of the lips, the left eye, and the right eye (m^2).

Figure 9 shows the calculation for the administered dose index for each particle size. The difference in the doses administered to the left eye and right eye is less obvious, so the difference between the eyes in Figure 8 more likely comes from the surface area, which varies among subjects. Generally speaking, lips had the largest administered dose for particles between 0.6 and 5.0 μm. When the particle size was less than 1.0 μm, the dose to the lips was only 1.28 times that of the eyes. As the particle size increased, the ratio also showed a significant increase. For

particles larger than 3.0 μm, the administered dose indexes of the eyes and lips were 30.7 ± 5.66 × 10^{-4} mg/m^2· s and 83.40 ± 4.39 ×10^{-4} mg/m^2· s, respectively. Particle deposition on the lips was 2.55 times that on the eyes, and the figure increased to 3.22 with the use of 5-μm particles. The results reveal that the lips have a greater exposure risk, especially with large particles.

3.3 Influence of inhalation airflow

We measured the administered dose of various particle sizes without inhalation to quantify the effect of inhalation airflow. All parameters were the same as those listed in Table 1 except that the pump was turned off.

P_i indicates the administered dose of the eyes and lips (w_i) to the dose of the total facial mucosa (w). Figure 10 shows the results,

$$P_i = \frac{w_i}{w} \quad (1)$$

Where

P_i is the deposition percentage of the left eye (P_{le}), right eye (P_{re}), and lips (P_l) (%);

w_i is the administered dose on the left eye (w_{le}), right eye (w_{re}), and lips (w_l) (g);

w is the administered dose on the total facial mucosa, $w = w_{le} + w_{re} + w_l$ (g).

The influence of inhalation airflow increased as the particle size decreased. For particles between 0.6 and 2.0 μm, the influence of inhalation airflow was less than 5.0%, but for 3.0-μm and 5.0-μm particles, the ratio dropped below 1.0%. Because the sink flow into the mouth has little effect on the airflow field outside the mouth, inhalation airflow may not be necessary to measure mucosal deposition of large particles near their source.

4. Discussion

The mucosal surface is susceptible because its barriers are less effective than those of intact skin[9]. Although mucosa lining fluid can compensate and trap some foreign particles with its adhesive and viscoelastic layers, others may penetrate the mucosa into the human circulatory system.

The published clinical studies can help to understand the response of the mucosal dose to particulate contaminants. Chu et al. found a significant connection between the $PM_{2.5}$ concentration and oral cancer based on a large sample size[6]. Exposure to heavy metal pollutants such as arsenic, nickel, and chromium increases the risk of oral cancer. Veres[4] concluded that inhaled environmental allergens may induce aberrant activation of immune cells in the airway mucosa, resulting in allergic airway disease. Studies of the side effects of drug delivery have also shown that penetration of particulates through mucus poses a potential risk to human health[12]. Nanocarriers are normally used in drug delivery because they can penetrate quickly through mucus to reach the underlying cells. Takeuchi et al. believed that particle size plays an important role in particle movement in mucus[47]. They examined the ability of chitosan-coated liposomes to penetrate mucus after oral administration of liposomes in rats. Their results showed that 100-nm liposomes had the best penetration ability. Hadrup et al. [9] discussed the toxicity of nanoparticles after dermal and mucosal surface exposure. Exposure to silver particles can cause localized argyria and eye irritation, and a 7-g dose of silver nitrate (~64 mg silver/kg body weight) is fatal to humans.

The administered doses on eyes and lips in our experimental setup were much lower than the fatal dose reported by Hadrup et al.[9], and the particle concentrations in our experiment could be much lower than those in the actual industrial environment under a specific production process. The average concentration during arc welding is 1.42×10^7 particles/cm^3 at 4.8 cm from the emission source[48]. This is 3.5 million times higher than the concentration in our experiment (4.0 particles per cm^3). Welding particles, mostly between 14 nm and 10 μm, are highly toxic heavy metals[49]. Measurements by Zimmer and Biswas revealed that the average particle concentration in breathing zone during welding can reach 5 mg/m^3 [48]. The dose thus administered to the facial mucosa during welding may cause significant damage if the workers fail to use effective protection.

Exposure to 5 μg/m^3 of particles between 1.0 and 7.0 μm can increase irritation in the eyes, nose, and throat[7]. Long-term exposure to such particulate contaminants increases mucosa

permeability and makes penetration of the mucus a more effective pathway. More studies are needed to determine the chronic health effects after long-term mucosa exposure.

One important influence on the administered dose is the proximity to the source. In our study, the distance between the susceptible individual and the particle source was 0.2 m, which falls within the range of the direct deposition route or the short-range airborne route, if the source is an index patient with a respiratory infection like tuberculosis or influenza[50]. In our measurements, particles between 0.6 and 5.0 μm may represent the expiratory aerosols that carry influenza viruses[51]. The particle-laden jet is also similar to a snapshot of the coughing or breathing airflow from the host of a pathogen, when the puff flow is fully developed[52]. Our results indicate that mucosal deposition acts as an important pathway, especially for particles with larger sizes in terms of dosage. Nevertheless, the viability of pathogens after deposition on facial mucosa may be challenged by factors such as the sharp temperature decrease in the expired droplets, impaction upon deposition, and defense proteins in the mucus[53]. Detailed studies that include actual pathogens or their surrogates such as bacteriophages could help us understand some of these complexities.

In addition to mucosal deposition, inhalation exposure is also an important exposure route. We plan to further quantify the inhalation exposure of airborne particles based on the workbench of this study. Although our model includes neither epithelial cells to absorb particles nor cilia to activate the mucus clearance mechanism, we aim to compensate with existing theoretical and anatomical models to calibrate compartmental deposition along the airway. Because lower airway exposure contributes to most health risks, the overall administered dose of particles that penetrate the lower airway from the sixth generation of the bronchi will be measured. When compared to the administered dose on the facial mucosa, the relative importance of the lower airway exposure route and the mucosal exposure route will become evident.

5. Conclusions

This study introduced a method to quantify the administered dose of particles deposited on the facial mucosa. A realistic face and airway model that includes a face, an oropharynx, a trachea, the first five generations of bronchi, and lung volume was fabricated via CT scanning and 3D

printing techniques. By simulating a mouth-breather with 11.0 ± 1.0 L/min continuous inhalation airflow, we quantified the administered dose as monodispersed fluorescent particles released from an incoming jet located 0.2 m from the nose.

Approximately 1.0% to 2.0% of the released micron-sized particles were deposited on the model's eyes and lips, and 0.6-μm, 3.0-μm, and 5.0-μm particles showed higher deposition rates than 1.0-μm and 2.0-μm particles. More than 80% of the total administered dose was deposited on the facial mucosa rather than on the eyes. Our in vitro realistic face and airway model does not include the biological features of real human subjects, but it can help to quantify the administered dose of particles with decent accuracy. This method is a convenient and economical means to test safety zones and protection methods with actual doses from a nearby pollutant source.

References

1. Stanaway JD, Afshin A, Gakidou E, et al. Global, regional, and national comparative risk assessment of 84 behavioural, environmental and occupational, and metabolic risks or clusters of risks for 195 countries and territories, 1990–2017: A systematic analysis for the Global Burden of Disease Study 2017. *The Lancet*. 2018;392(10159):1923-1994.

2. International Newsletter on Occupational Health and Safety 2018; The International Labour Office (ILO), *Special Issue*, 1-31.

3. Sexton K, Callahan MA, Bryan EF. Estimating exposure and dose to characterize health risks: The role of human issue monitoring in exposure assessment. *Environ Health Perspect*. 1995;103:17.

4. Veres TZ. Visualizing immune responses of the airway mucosa. *Cell Immunol*. 2018. In press.

5. Ban S, Suzuki S, Kubota K, et al. Gastric mucosal status susceptible to lanthanum deposition in patients treated with dialysis and lanthanum carbonate. *Ann Diagn Pathol*. 2017;26:6-9.

6. Chu YH, Kao SW, Tantoh DM, et al. Association between fine particulate matter and oral cancer among Taiwanese men. *J Investig Med*. 2019;67(1):34-38.

7. Wolkoff P. External eye symptoms in indoor environments. *Indoor Air*. 2017;27(2):246-260.

8. Klen J, Wolkoff P. Changes in eye blink frequency as a measure of trigeminal stimulation by exposure to limonene oxidation products, isoprene oxidation products and nitrate radicals. *Int Arch Occup Environ Health*. 2004;77(4):235-243.

9. Hadrup N, Sharma AK, Loeschner K. Toxicity of silver ions, metallic silver, and silver nanoparticle materials after in vivo dermal and mucosal surface exposure: A review. *Regul Toxicol Pharmacol*. 2018;98:257-267.

10. Wolkoff P. Eye complaints in the office environment: Precorneal tear film integrity influenced by eye blinking efficiency. *Occup Environ Med*. 2005;62(1):4-12.

11. Dorrani M, Kaul M, Parhi A, et al. TXA497 as a topical antibacterial agent: Comparative antistaphylococcal, skin deposition, and skin permeation studies with mupirocin. *Int J Pharm*. 2014;476(1-2):199-204.

12. Lock JY, Carlson TL, Carrier RL. Mucus models to evaluate the diffusion of drugs and particles. *Adv Drug Deliv Rev*. 2018;124:34-49.

13. Kanashova T, Sippula O, Oeder S, et al. Emissions from a modern log wood masonry heater and wood pellet boiler: Composition and biological impact on air-liquid interface exposed human lung cancer cells. *J Mol Clin Med*. 2018;1.

14. Hougaard KS, Jackson P, Kyjovska ZO, et al. Effects of lung exposure to carbon nanotubes on female fertility and pregnancy. A study in mice. *Reprod Toxicol Elmsford N*. 2013;41:86-97.

15. Shen LN, Zhang YT, Wang Q, et al. Enhanced in vitro and in vivo skin deposition of apigenin delivered using ethosomes. *Int J Pharm*. 2014;460(1-2):280-288.

16. Day DB, Xiang J, Mo J, et al. Association of ozone exposure with cardiorespiratory pathophysiologic mechanisms in healthy adults. *JAMA Intern Med*. 2017;177(9):1344.

17. Rich DQ, Kipen HM, Huang W, et al. Association between changes in air pollution levels during the Beijing Olympics and biomarkers of inflammation and thrombosis in healthy young adults. *JAMA*. 2012;307(19).

18. Gemci T, Ponyavin V, Chen Y, et al. Computational model of airflow in upper 17 generations of human respiratory tract. *J Biomech*. 2008;41(9):2047-2054.

19. Xu XY, Ni SJ, Fu M, et al. Numerical investigation of airflow, heat transfer and particle deposition for oral breathing in a realistic human upper airway model. *J Therm Biol*. 2017;70:53-63.

20. Qi S, Zhang B, Teng Y, et al. Transient dynamics simulation of airflow in a CT-scanned human airway tree: More or fewer terminal bronchi? *Comput Math Methods Med*. 2017;1-14.

21. Koullapis PG, Kassinos SC, Bivolarova MP, Melikov AK. Particle deposition in a realistic geometry of the human conducting airways: Effects of inlet velocity profile, inhalation flowrate and electrostatic charge. *J Biomech*. 2016;49(11):2201-2212.

22. Paxman T, Noga M, Finlay WH, Martin AR. Experimental evaluation of pressure drop for flows of air and heliox through upper and central conducting airway replicas of 4- to 8-year-old children. *J Biomech*. 2019;82:134-141.

23. Lizal F, Elcner J, Hopke PK, et al. Development of a realistic human airway model. *Proc Inst Mech Eng [H]*. 2012;226(3):197-207.

24. Kaczmarczyk J, Melikov A, Bolashikov Z, et al. Human response to five designs of personalized ventilation. *HVACR Res*. 2006;12(2):367-384.

25. Ou C, Deng Q, Liu W. Numerical simulation of particle deposition in obstructive human airways. *J Cent South Univ*. 2012;19(3):609-614.

26. Frederix EMA, Kuczaj AK, Nordlund M, et al. Simulation of size-dependent aerosol deposition in a realistic model of the upper human airways. *J Aerosol Sci*. 2018;115(Supplement C):29-45.

27. Islam MS, Saha SC, Sauret E, et al. Pulmonary aerosol transport and deposition analysis in upper 17 generations of the human respiratory tract. *J Aerosol Sci*. 2017;108:29-43.

28. Wei J, Tang JW, Borojeni AAT, et al. Low re-inhalation of the exhaled flow during normal nasal breathing in a pediatric airway replica. *Build Environ*. 2016;97:40-47.

29. Brown JS, Gordon T, Price O, Asgharian B. Thoracic and respirable particle definitions for human health risk assessment. *Part Fibre Toxicol*. 2013;10(1):12.

30. Adams WC. Measurement of breathing rate and volume in routinely performed daily activities: Final Report, *Contract.* 1993.

31. Da G, Géhin E, Ben-Othmane M, et al. An experimental approach to measure particle deposition in large

circular ventilation ducts. *Environ Sci Pollut Res*. 2015;22(7):4873-4880.

32. Aumond S, Bitton E. The eyelash follicle features and anomalies: A review. *J Optom*. 2018;11(4):211-222.

33. Amador GJ, Mao W, DeMercurio P, et al. Eyelashes divert airflow to protect the eye. *J R Soc Interface*. 2015;12(105):20141294.

34. Levy Y, Segal N, Ben-Amitai D, Danon YL. Eyelash length in children and adolescents with allergic diseases. *Pediatr Dermatol*. 2004;21(5):534-537.

35. Liu M, Zhang J, Shan W, Huang Y. Developments of mucus penetrating nanoparticles. *Asian J Pharm Sci*. 2015;10(4):275-282.

36. Lai SK, O'Hanlon DE, Harrold S, et al. Rapid transport of large polymeric nanoparticles in fresh undiluted human mucus. *Proc Natl Acad Sci U S A*. 2007;104(5):1482-1487.

37. Witten J, Ribbeck K. The particle in the spider's web: Transport through biological hydrogels. *Nanoscale*. 2017;9(24):8080-8095.

38. White MR, Helmerhorst EJ, Ligtenberg A, et al. Multiple components contribute to ability of saliva to inhibit influenza viruses. *Oral Microbiol Immunol*. 2009;24(1):18-24.

39. Fábián TK, Hermann P, Beck A, et al. Salivary defense proteins: Their network and role in innate and acquired oral immunity. *Int J Mol Sci*. 2012;13(4):4295-4320.

40. Xiong R, Wu Q, Trbojevich R, et al. Disease-related responses induced by cadmium in an in vitro human airway tissue model. *Toxicol Lett*. 2019;303:16-27.

41. Li S, Xie J, Dong M, Bai L. Rebound characteristics for the impact of SiO_2 particle onto a flat surface at different temperatures. *Powder Technol*. 2015;284:418-428.

42. Tang JW, Noakes CJ, Nielsen PV, et al. Observing and quantifying airflows in the infection control of

aerosol- and airborne-transmitted diseases: An overview of approaches. *J Hosp Infect*. 2011;77(3):213-222.

43. Licina D, Melikov A, Pantelic J, et al. Human convection flow in spaces with and without ventilation: Personal exposure to floor-released particles and cough-released droplets. *Indoor Air*. 2015;25(6):672-682.

44. Rim D, Novoselac A. Occupational exposure to hazardous airborne pollutants: Effects of air mixing and source location. *J Occup Environ Hyg*. 2010;7(12):683-692.

45. Voelker C, Alsaad H. Simulating the human body's microclimate using automatic coupling of CFD and an advanced thermoregulation model. *Indoor Air*. 2018;28(3):415-425.

46. Awbi HB. Ventilation of Buildings, 2nd ed. 2003.

47. Netsomboon K, Bernkop-Schnürch A. Mucoadhesive vs. mucopenetrating particulate drug delivery. *Eur J Pharm Biopharm*. 2016;98:76-89.

48. Zimmer AT, Biswas P. Characterization of the aerosols resulting from arc welding processes. *J Aerosol Sci*. 2001;32(8):993-1008.

49. Stephenson D, Seshadri G, Veranth JM. Workplace exposure to submicron particle mass and number concentrations from manual arc welding of carbon steel. *AIHA J*. 2003;64(4):516-521.

50. Liu L, Li Y, Nielsen PV, Wei J, Jensen RL. Short-range airborne transmission of expiratory droplets between two people. *Indoor Air*. 27(2):452-462.

51. Yan J, Grantham M, Pantelic J, et al. Infectious virus in exhaled breath of symptomatic seasonal influenza cases from a college community. *Proc Natl Acad Sci*. 2018;115(5):1081-1086.

52. Wei J, Li Y. Human cough as a two-stage jet and its role in particle transport. Gurka R, ed. *PLOS ONE*. 2017;12(1):e0169235.

53. Tang JW, Gao CX, Cowling BJ, et al. Absence of detectable influenza RNA transmitted via aerosol during

various human respiratory activities – Experiments from Singapore and Hong Kong. Bouvier NM, ed. *PLoS ONE*. 2014;9(9):e107338.

Tables

Table 1 Experimental parameters.

Particle diameter (μm)	Density (kg/m^3)	Exposure time (min)	Breath type	Flow rate (L/min)
0.6	1530	50	Mouth-breather	11.0 ± 1.0
1.0		40		
2.0		30		
3.0		20		
5.0		10		

Table 2 Relationship between L/W and fluorescence intensity $\overline{\Delta I}$.

	L/*W*	0.0	0.1	0.2	0.4	0.8
$\overline{\Delta I}$	Amador (2015)[33] (10-μm droplets, *Re* = 500-1000)	1.0 ± 0.2	0.8 ± 0.1	0.4 ± 0.2	0.8 ± 0.1	1.2 ± 0.2
	Current study (0.6-μm to 5-μm particles, *Re* = 1500, *W* = 26.74 mm)	Face and airway model	Animal	Animal and human *L* = 8 to 12 mm[34]; *L*/*W* = 0.3 to 0.5; $\overline{\Delta I}$ = 0.6 to 0.9		Animal

Figure legends

Fig. 1. Segmentation process of computed tomographic images. a: single slice of computed tomographic scan; b: segmented face, nasal, throat, airway, and lung volumes; and c: completed realistic face and airway model.

Fig. 2. Three-dimensional printed in vitro face and airway model.

Fig. 3. Experimental setup for human exposure assessment.

Fig. 4. Fluorescence intensity–mass concentration standard curves in various concentration distributions.

Fig. 5. Benchmark measurement of fluorescence on blank surfaces and within pure water droplets.

Fig. 6. Background fluorescence intensity measurement.

Fig. 7. Total mass of generated particles for various particle sizes.

Fig. 8. Mucosal deposition rate versus particle size [mucosal administered dose (g) / generated particle mass (g)]

Fig. 9. Administered dose index versus particle size.

Fig. 10. Deposition percentage for particles of various diameters with and without inhaled airflow.

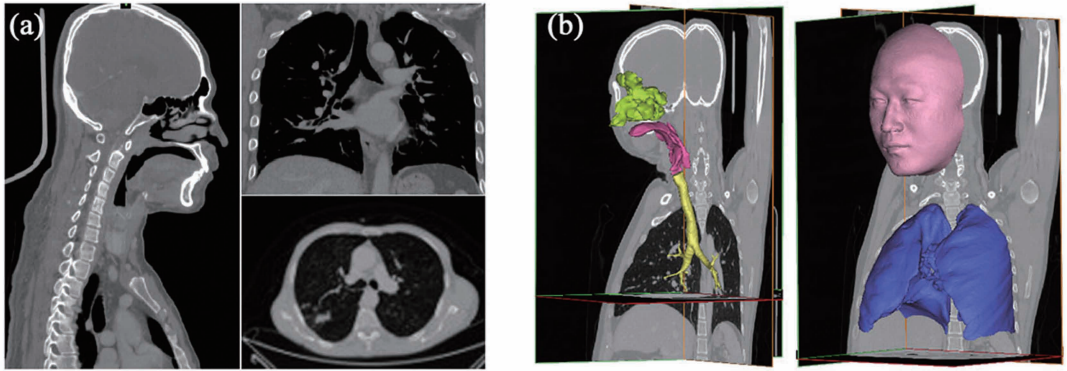
(a)
(b)
(c)

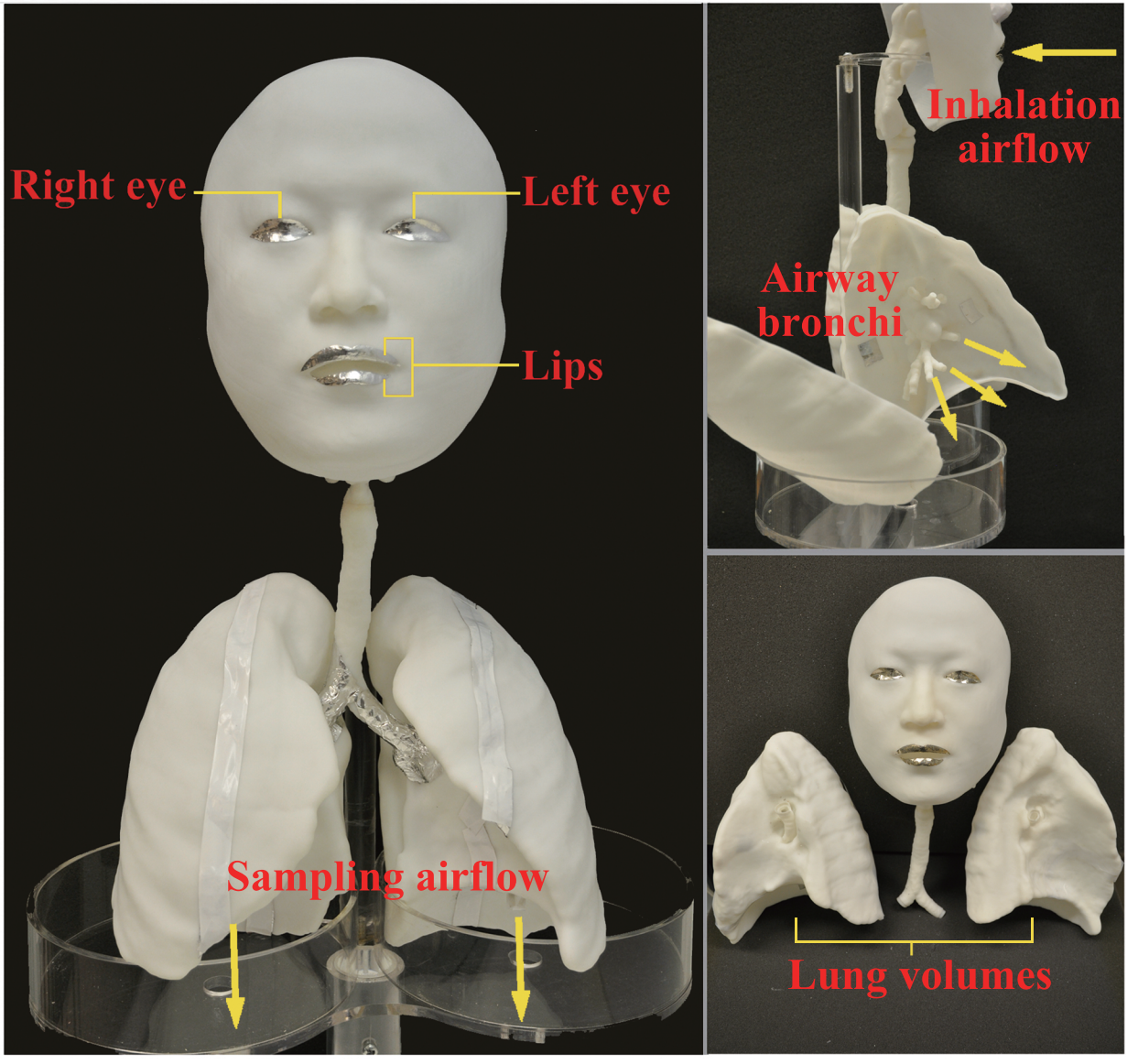
Right eye
Left eye
Lips
Sampling airflow
Inhalation airflow
Airway bronchi
Lung volumes

APS

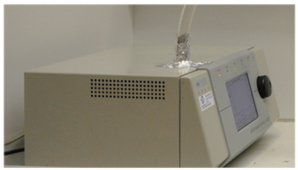

Monodispersed particle jet
0.6 - 5.0 µm
Monodispersity 78.5%~93.3%

VOAG

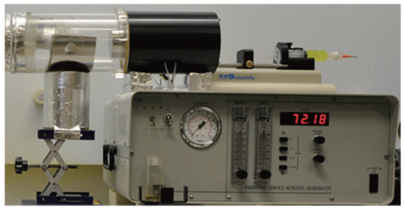

Human replica

20 cm

Jet opening:
Φ = 0.04 m

Air velocity:
v = 0.94 m/s

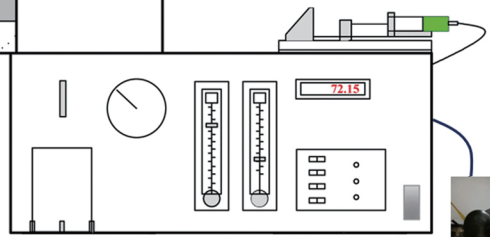

Air compressor

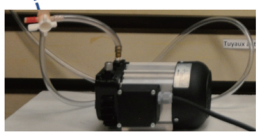

Pump
11.0 ± 1.0 L/min

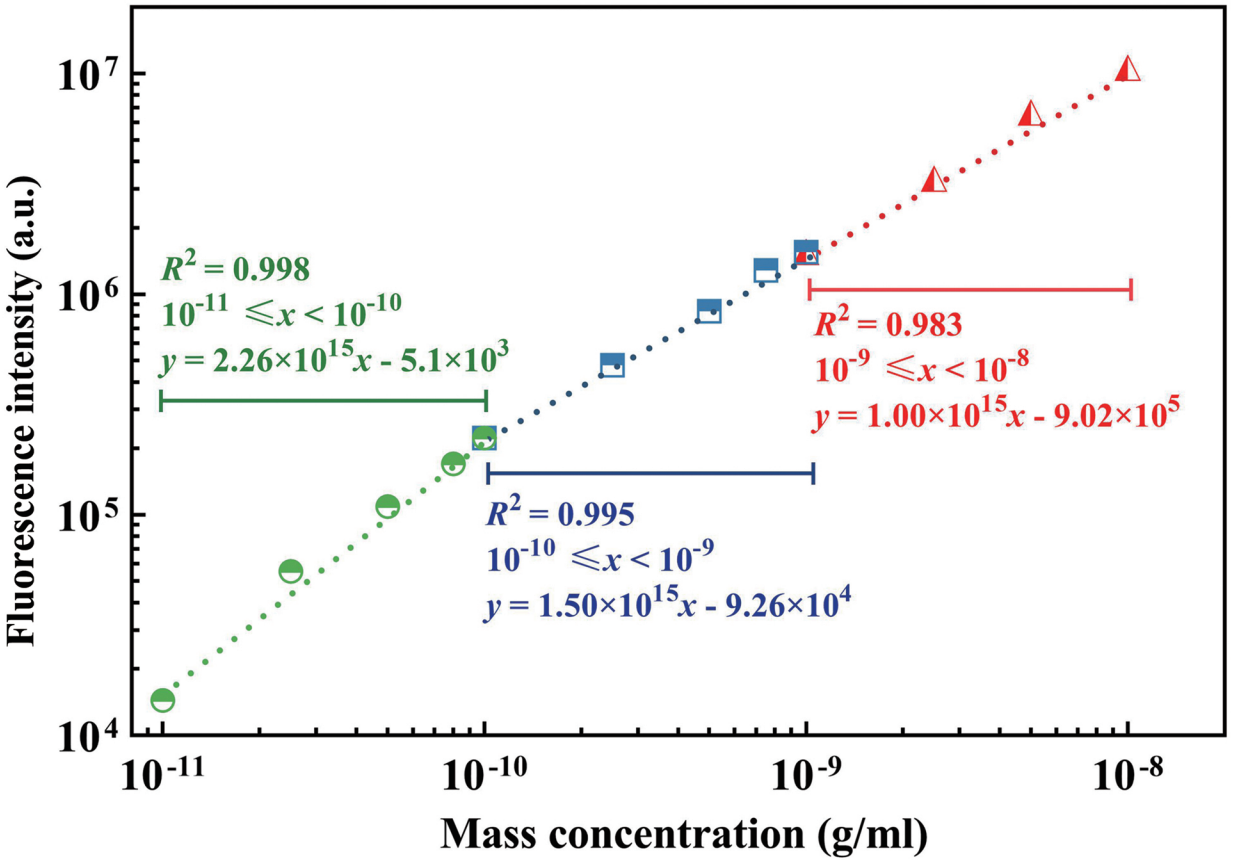
Fluorescence intensity (a.u.)
10^7
10^6
10^5
10^4
10^{-11}
10^{-10}
10^{-9}
10^{-8}
Mass concentration (g/ml)
$R^2 = 0.998$
$10^{-11} \leqslant x < 10^{-10}$
$y = 2.26\times10^{15}x - 5.1\times10^3$
$R^2 = 0.995$
$10^{-10} \leqslant x < 10^{-9}$
$y = 1.50\times10^{15}x - 9.26\times10^4$
$R^2 = 0.983$
$10^{-9} \leqslant x < 10^{-8}$
$y = 1.00\times10^{15}x - 9.02\times10^5$

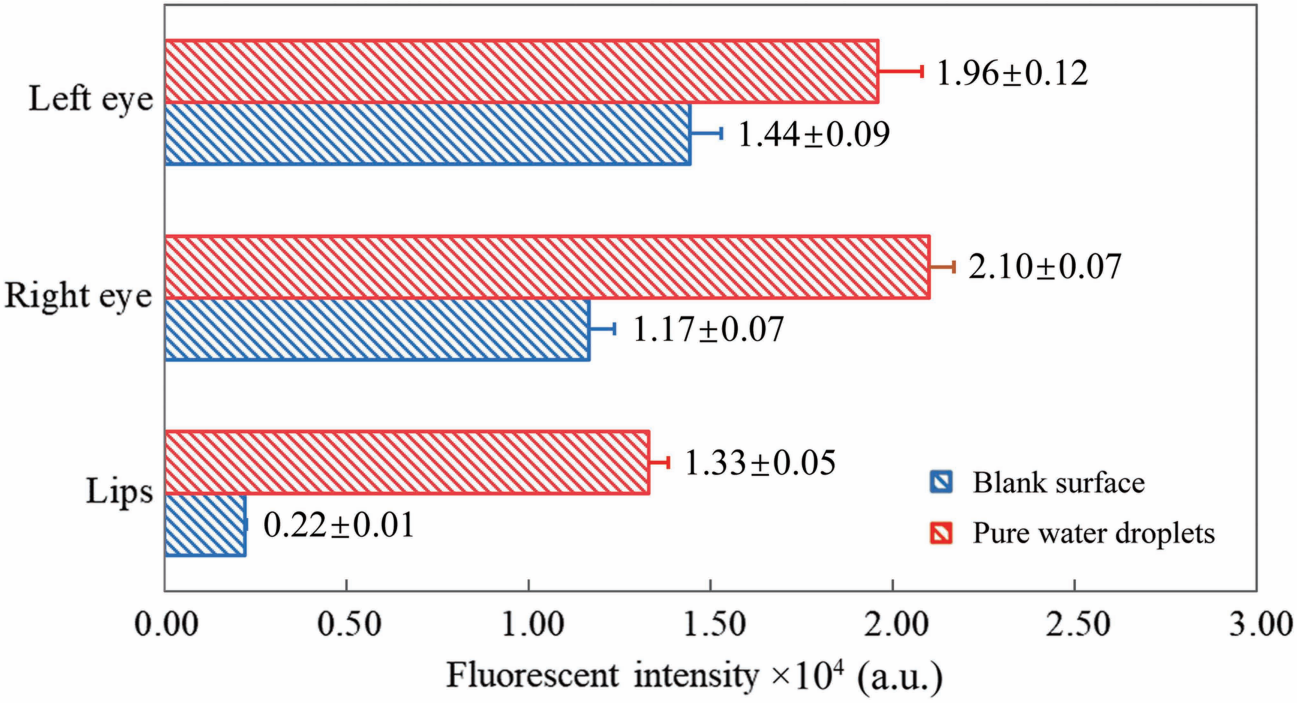
Left eye
Right eye
Lips
1.96±0.12
1.44±0.09
2.10±0.07
1.17±0.07
1.33±0.05
0.22±0.01
Blank surface
Pure water droplets
0.00
0.50
1.00
1.50
2.00
2.50
3.00
Fluorescent intensity ×10⁴ (a.u.)

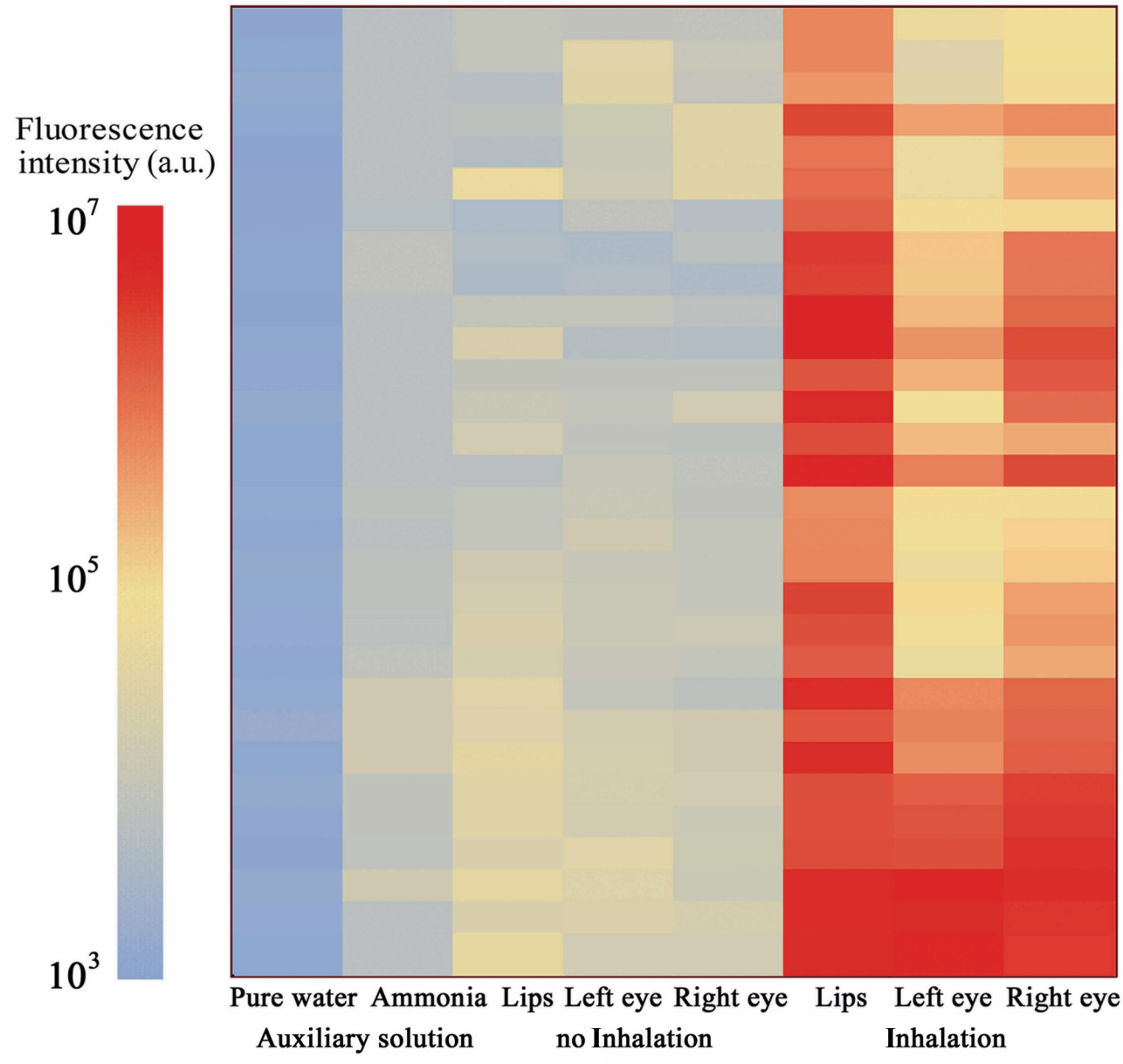
Fluorescence intensity (a.u.)
10^7
10^5
10^3
Pure water
Ammonia
Lips
Left eye
Right eye
Lips
Left eye
Right eye
Auxiliary solution
no Inhalation
Inhalation

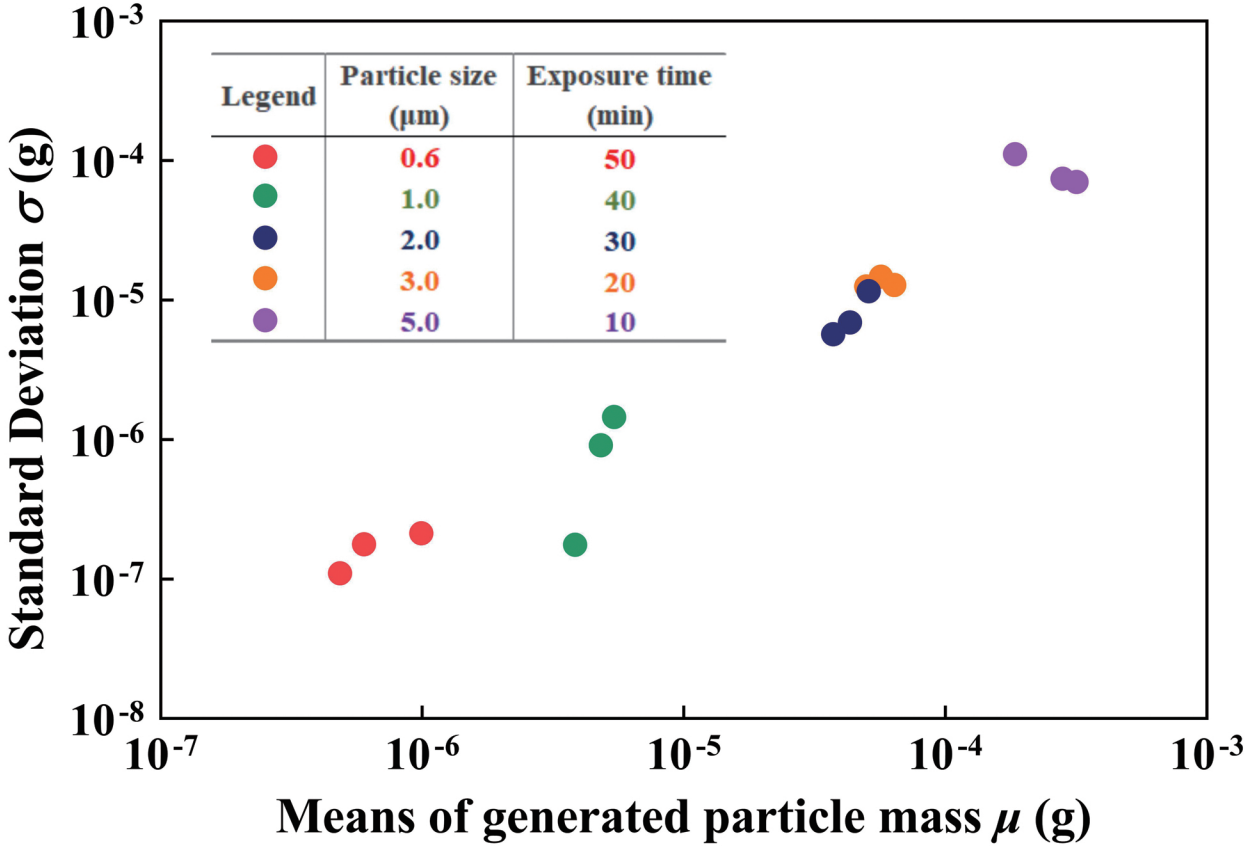
Legend
Particle size (μm)
Exposure time (min)
0.6
50
1.0
40
2.0
30
3.0
20
5.0
10
Standard Deviation σ (g)
Means of generated particle mass μ (g)
10-3
10-4
10-5
10-6
10-7
10-8
10-7
10-6
10-5
10-4
10-3

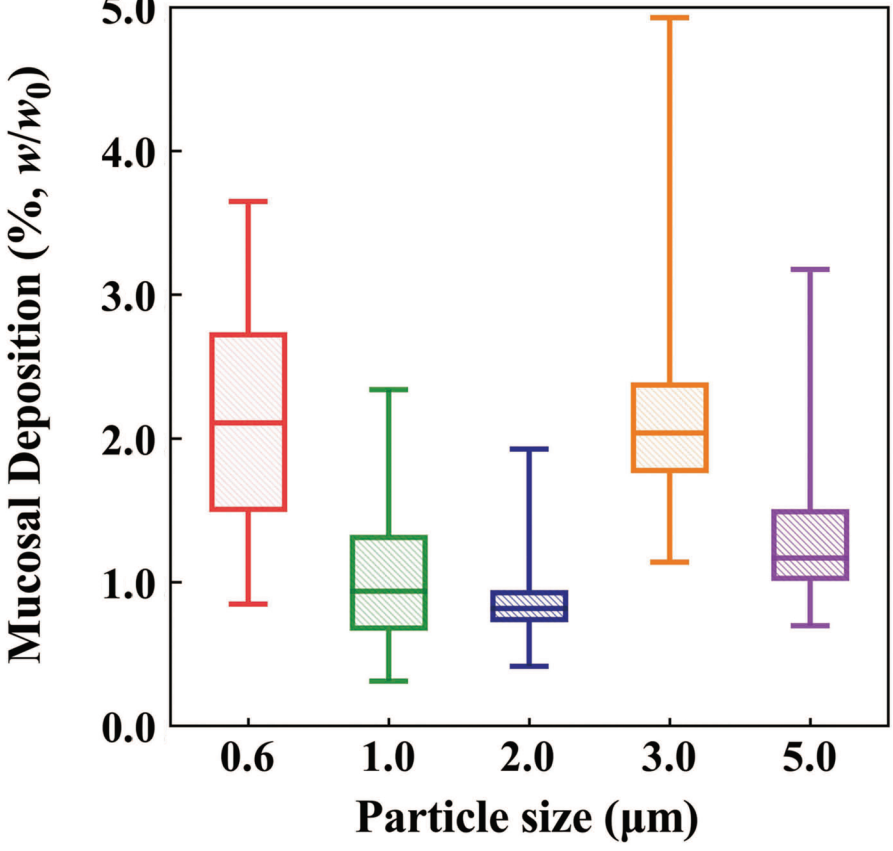

Particle size (μm)	Left eye (%)	Right eye (%)	Lips (%)
0.6	0.17	0.28	1.70
1.0	0.03	0.33	0.66
2.0	0.02	0.09	0.76
3.0	0.07	0.18	1.88
5.0	0.05	0.09	1.40

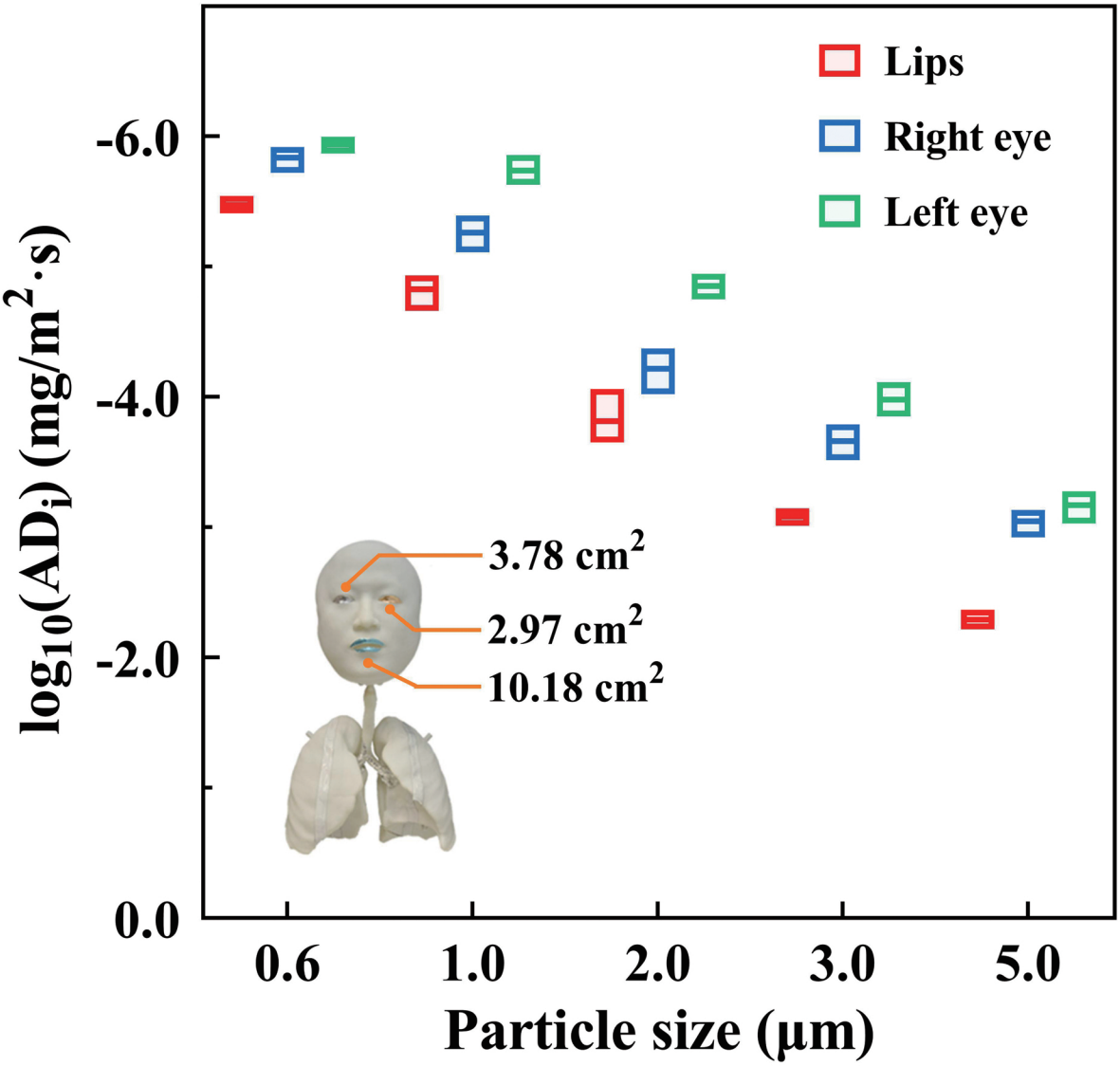
Lips
Right eye
Left eye
-6.0
-4.0
-2.0
0.0
$\log_{10}(AD_i)$ (mg/m^2·s)
3.78 cm^2
2.97 cm^2
10.18 cm^2
0.6
1.0
2.0
3.0
5.0
Particle size (μm)

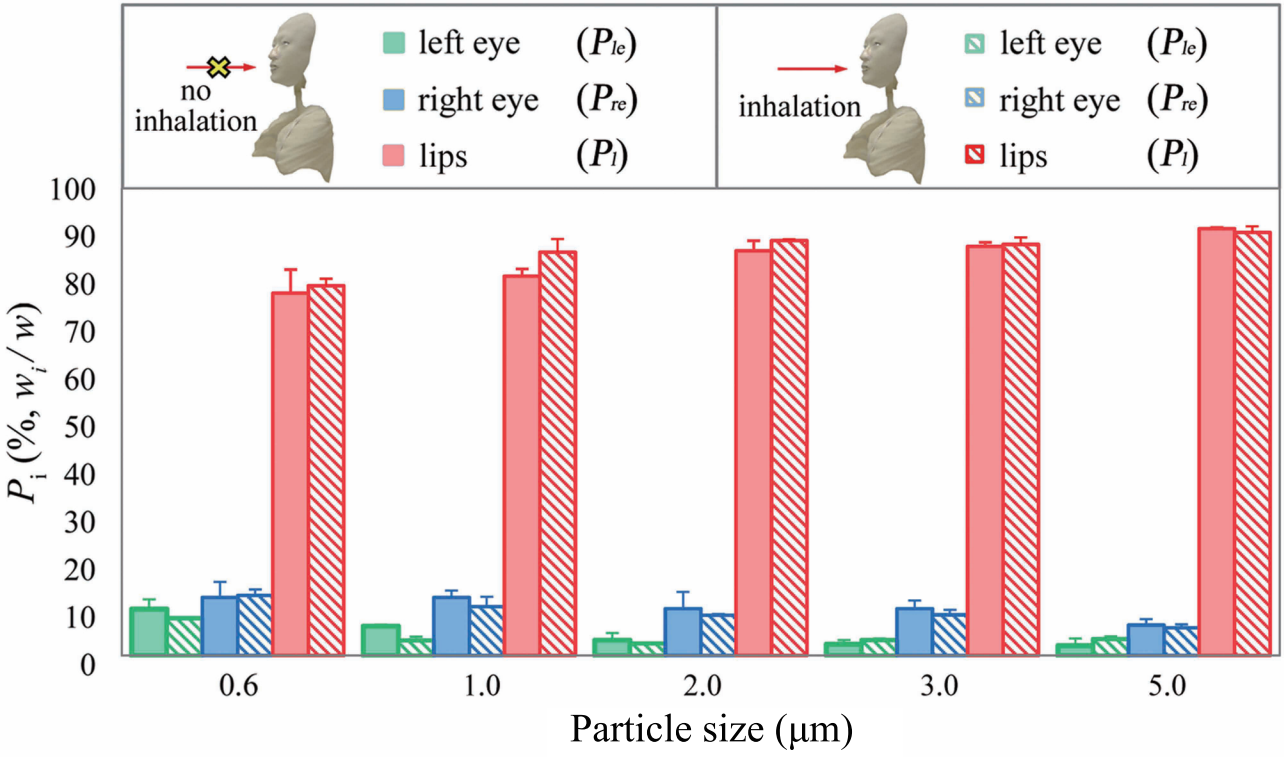
no inhalation
left eye (P_{le})
right eye (P_{re})
lips (P_l)
inhalation
left eye (P_{le})
right eye (P_{re})
lips (P_l)
P_i (%, w_i / w)
100
90
80
70
60
50
40
30
20
10
0
0.6
1.0
2.0
3.0
5.0
Particle size (μm)